https://doi.org/10.1016/j.ijmecsci.2018.03.019

Theoretical and experimental investigation into non-uniformity of surface generation in micro-milling

Zhanwen Sun[a], Suet To[a,*], Shaojian Zhang[a], and Guoqing Zhang[b]

[a] *State Key Laboratory of Ultra-precision Machining Technology, Department of Industrial and Systems Engineering, The Hong Kong Polytechnic University, Hong Kong, PR China*

[b] *Guangdong Provincial Key Laboratory of Micro/Nano Optomechatronics Engineering, College of Mechatronics and Control Engineering, Shenzhen University, Shenzhen, Guangdong, PR China*

**Corresponding author at: The Hong Kong Polytechnic University, Department of Industrial and Systems Engineering, State Key Laboratory in Ultra-precision Machining Technology, Kowloon, Hong Kong. Email：* sandy.to@polyu.edu.hk*; Tel: +852 2766 6587; Fax: +852 2764 7657*

Abstract

Surface quality is significantly affected by the special cutting mechanisms in micro-milling, which include the effects of minimum chip thickness and ploughing. The uncut chip thickness changing with tool rotation varies the cutting mechanisms further to make surface generation non-uniform. However, there is currently no evaluation methods and prediction models for the non-uniformity of micro-milled surface quality. In this paper, a relative standard deviation of surface roughness (RSDS) method is developed to evaluate micro-milled surface non-uniformity, and its effectiveness is statistically demonstrated. Additionally, a mathematical model that considers alignment errors, relative tool sharpness (RTS), material elastic recovery and ploughing effect is proposed to estimate surface non-uniformity. Theoretical and experimental results reveal that: (i) the variation of surface generation mechanisms can induce periodic cutting force oscillations and surface non-uniformity; (ii) non-uniform surfaces exhibit low surface roughness with shearing in the center and high surface roughness with ploughing on the sides; (iii) feed rate determines the shearing interval length and depth of cut makes significant impact upon average surface roughness; and (iv) RSDS can effectively evaluate surface non-uniformity and the proposed model well predicts surface non-uniformity. The research furthers the understanding of surface generation mechanism with surface quality prediction and machining parameter optimization in micro-milling.

Keywords: Micro-milling, Ploughing effect, Surface generation mechanisms, Relative tool sharpness

Nomenclature		N	The number of the discrete regions
(x_c^i, y_c^i)	Coordinates of tool edge center in the direction of φ_i	A_t^i	The total volume of tool contact material in the direction of φ_i

x_j	The coordinate of the j-th point in feed direction	A_s^i, A_p^i	The volume of sheared and ploughed material in the direction of φ_i
φ_i	The i-th tool rotation angle	r_o	Tool runout length
γ_i	Instantaneous negative rake angle	δ	Tool runout angle
h_i	The instantaneous uncut chip thickness in the direction of φ_i	NSPA_i	The i-th normal specific ploughing amount
h_{min}	Minimum chip thickness	$\hat{n}(x_j)$	Normal vector along the tool edge
h_{max}	Maximum uncut chip thickness	$\delta(x_j)$	Correction coefficient
Ra_i	The surface roughness of the i-th discrete region	K, n	Material related coefficients
		z_e^{ij}	The height of tool edge profile
Ra_g^i	Geometric surface roughness in the direction of φ_i	h_e^{ij}	The elastic recovery height in the direction of φ_i and at x_j
Ra_s^i	Stochastic surface roughness in the direction of φ_i	z_{ij}	The height of the residual tool marks in the direction of φ_i and at x_j
μ	Average value of N discrete surface roughness	f_t	Feed per tooth
		d	Depth of cut
σ	Standard deviation of N discrete surface roughness	n	Spindle rotation speed
		R	The normal radius of the milling tool
ρ	Elastic recovery coefficient	α	Tool clearance angle
n_f	The ordinal number of tool flutes	r_e	Tool edge radius
M	Sampling points in calculating Ra_i		

1. Introduction

Because of the ability to fabricate complex micro 3D features on various kinds of metallic and nonmetallic materials, the application of micro-milling technology to the fabrication of micro components has received extensive attention from researchers and designers [1]. However, the surface generation mechanism in micro-milling is different from macro-milling due to the comparative size between tool edge radius and uncut chip thickness. The relative blunt tool sharpness in micro-milling results in special cutting mechanisms such as minimum chip thickness effect [2], large negative rake angle [3], ploughing [4], size effect [5, 6] and runout [7]. Based on the machining conditions and the

stiffness of the experiment setup, some or all of these special cutting mechanisms may dominate the surface generation during micro-milling. As a result, the analysis of micro-milled surface quality cannot be understood simply by downscaling from macro-milling.

Because of the kinematic characteristics of micro-milling, the rotation track of milling flutes can induce periodic variation of the uncut chip thickness. As the surface generation mechanism in micro-milling is significantly determined by the size of uncut chip thickness, the dominant surface generation mechanism in the center of the micro-milled slots can be totally different from that on the sides. The parameter normally used to identify the different surface generation mechanisms is relative tool sharpness (RTS), which is defined as the ratio of the uncut chip thickness to the tool edge radius [8]. The relationship between RTS and surface generation mechanisms was studied by Rahman et al. [9] through conducting orthogonal cutting experiments on Mg and Cu alloy. It was concluded that with the decrease of RTS value, the material remove mechanism gradually transformed from shearing to extrusion to ploughing and rubbing. Through observing the cutting force signals, the interchanging shearing and ploughing mechanisms were also demonstrated in micro-slot milling by Filiz et al. [10]. The shape of the cutting force signals below the minimum chip thickness is similar to that when indenting the workpiece material, while the forces switched to shearing forces when the RTS exceeding a critical value. Therefore, the generation of micro-milled surfaces belongs to a dynamic process, with different surface generation mechanisms dominating at different values of uncut chip thickness. However, the variation of surface generation mechanisms and its effect on micro-milled surface non-uniformity are not fully understood.

The difference in the quality of micro-milled surfaces along the tool-rotating track was most notably discussed by Ramos et al. [4] who concluded that the non-uniform surface roughness and burr size is related to the periodically changed surface generation mechanisms from ploughing to shearing. Based on the changes in the ploughing marks and residual stresses, the transformation of the surface generation mechanisms between micro and macro was demonstrated. Similar results were also found in the milling of brittle materials such as glass and silicon [11, 12]. It was concluded that ductility is dominant at low cutting thickness, but when the uncut chip thickness reaches the critical value for ductile-brittle transition, brittle fracture begins to take place. Overall, the variation of surface generation mechanisms is the main characteristic of micro-milling, which can induce generated surface non-uniformity. Consequently, there is a need to better understand the characteristics of the variation of

surface generation mechanisms and to investigate the evaluation methods of surface non-uniformity in micro-milling.

Several researchers have experimentally and theoretically investigated the factors influencing micro-milled surface quality. The effect of machining parameters on average surface roughness in micro-milling brass was discussed by Sooraj and Mathew [13], who concluded that the interaction of cutting speed and feed rate is critical in determining the bottom surface roughness. Through conducting experiments on Titanium alloy it was found that a higher feed rate provides a lower surface roughness in micro-milling, which is the opposite of macro-milling. Through finite element analysis of surface defects considering plastic dissipation energy, Simoneau et al. [14] found that material grain size affects surface roughness. A strong relationship between surface roughness and the homogeneity of the material microstructure was discovered by Uhmann et al. [15] when conducting micro-milling on sintered tungsten-copper composite materials. Amongst the foregoing investigations of factors influencing average surface roughness, there is none that investigates the factors affecting micro-milled surface non-uniformity.

At the same time, researchers were building mathematical surface generation models to estimate finished surface quality. A surface generation model was proposed by Vogler et al. [16] in consideration of the tool edge geometry and minimum chip thickness effect. The model simulated surface profile in the center of micro-milled slots further to estimate surface roughness. Based on Vogler's surface roughness model, a 3D surface generation model was developed by Liu et al. [17] to predict the surface topography on sidewall and floor surfaces. They divided the surface roughness model into a deterministic model, with a view to the process kinematics, alignment errors and dynamics, and a stochastic model that considered the ploughing effect and material elastic recovery; the material dependent coefficients in the model were acquired from experiment results. In addition, a mathematical model taking into consideration the workpiece material microstructure and the transformation of the cutting mechanisms at phase boundaries, was proposed by Abdelrahman et al. [18]. In their model, the workpiece material is clarified to be anisotropic, and the model can accurately predict the micro-burrs on the boundaries of the material phase. Even though exhaustive investigations have been conducted on micro-milled surface generation models, there has been little research into the effect of varying RTS on surface generation mechanisms and its induced surface non-uniformity. It is therefore necessary to develop a mathematical model that can be applied directly to the prediction of surface non-uniformity.

The variation of surface generation mechanisms and its induced non-uniform surfaces are the main characteristic of micro-milling. Nevertheless, there are no effective evaluation methods and prediction models for the non-uniformity of micro-milled surfaces, and the effect of machining parameters on surface non-uniformity is still unknown. In this paper, a relative standard deviation of surface roughness (RSDS) method is proposed to evaluate the non-uniformity of micro-milled surface. Additionally, a mathematical model is developed to estimate micro-milled surface non-uniformity and the distribution of surface roughness in cross-sectional direction. In the model, one-dimensional surface roughness is calculated discretely along the tool rotation angle in consideration of the changing relative tool sharpness (RTS). Through conducing Taguchi experiments and statistical analysis, the variation of surface generation mechanisms and its effect on surface non-uniformity at different machining parameters are discussed theoretically and experimentally.

2. Experimental setup

All the full-immersion slot micro-milling experiments were conducted on a 3-axis high-precision CNC micro-milling machine, provided by the Aerotech Company. The travel distance of X and Y slides was 300mm. The resolution and position accuracy were 0.01μm and 0.1μm respectively. A high-speed static gas pressure spindle was fixed on the Z slide with the highest rotating speed at 70,000 rpm. Two-flute uncoated carbide end milling tools with sharp-edges and 30° helix angle were used in the experiments. The normal diameter of the end milling tools was 1mm. Two replications were performed for each slot on two new workpieces.

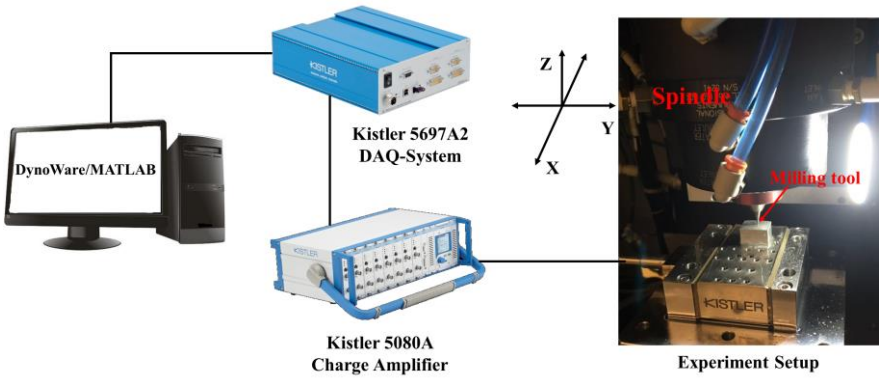

Fig. 1. Flowchart of cutting force signal measurement.

Micro-slots were parallelly machined on Al6061 workpieces with the width equal to the normal

diameter of the end milling tools. The X and Y slides carried a workpiece moving horizontally with a specific feed rate and the Z slide carried the spindle feeding vertically to cut at different depths of cut. Dry cutting was applied in the experiment to collect cutting force signals accurately. The cutting length of each slot and the cross-distance between two neighboring slots were appointed at 10mm and 4mm respectively.

A three-channel dynamometer sensor, Kistler 9256C1, was fixed between the X slide and the workpiece to capture the three orthogonal cutting force components (F_x, F_y and F_z). The analog signals of the cutting force components were collected by the dynamometer sensor Kistler 9256C1, then amplified by a Kistler 5080A charge amplifier and digitalized by a Kistler 5697A2 DAQ-System at a sampling frequency of 100,000 Hz. Afterwards, the cutting force data was analyzed by the DynoWare software and MATLAB software. The sketch map of cutting force measurement is shown in Fig. 1.

The workpieces were cleaned by alcohol after machining. The 3D topographies of the finished surfaces and surface roughness in the feed direction were acquired through employing an Optical Surface Profiler (Zygo Corporation, USA). According to EN ISO 4288, the sampling length and evaluation length of surface roughness measurement was 0.25mm and 1.25mm respectively to diminish the influence of the waviness profile. Additionally, a Hitachi TM3000 scanning electron microscope (SEM) was also used to observe ploughing marks on the milled surfaces.

Table 1. Machining parameters for Taguchi experiments.

Parameters	Values	Level
Spindle speed (rpm)	6000, 13500, 21000, 28500, 36000	5
Feed rate (μm/flute)	0.6, 1.2, 1.8, 2.4, 3	5
Depth of cut (μm)	10, 20, 30, 40, 50	5

Table 2. Cutting conditions.

The number of sampling points of surface roughness (N)	10
Tool runout length (r_o) (μm)	3
Tool runout angle (δ) (°)	50
Tool edge radius (r_e) (μm)	1.2
Tool clearance angle (α) (°)	10

In the designation of Taguchi based experiments, machining parameters (spindling speed, feed rate and depth of cut) were used as input variables. Spindle speed ranged from 6000rpm to 36000rpm, corresponding to low speed machining to high speed machining. Feed rate and depth of cut were chosen based on the recommendation from the literature and technicians, which ranges from 0.1μm/flute to 1.6μm/flute and 10μm to 50μm respectively. The machining parameters and the cutting condition are shown in Table 1 and Table 2, respectively. ANOVA and SN ratio analysis were conducted based on the experimental results. As the surface roughness and surface non-uniformity are the smaller-the-better, a lower-the-better quality characteristic was applied for the SN ratio analysis.

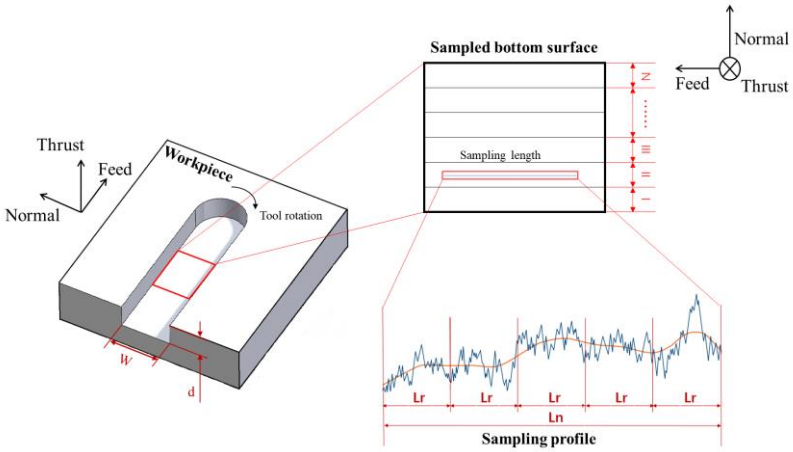

Fig. 2. Model for calculating RSDS.

3. Mathematical model

3.1 RSDS

To overcome the limitation of average surface roughness and area surface roughness in evaluating the non-uniformity of micro-milled surfaces, a relative standard deviation of surface roughness (RSDS) method is introduced in this section. The model for calculating RSDS is shown in Fig. 2. A micro-milled slot is equally divided into N sub-regions in the cross-sectional direction. Through separately measuring and comparing the profile surface roughness of the N sub-regions, the RSDS can be acquired. Specifically, RSDS is defined as the ratio of the standard deviation of the N profile surface roughness (σ) to the average surface roughness (μ). The average surface roughness (μ) is calculated by:

$$\mu = \frac{1}{N}\sum_{i=1}^{N} Ra_i \tag{1}$$

where Ra_i is the i-th profile surface roughness of the N divided sub-regions. The standard deviation

of the N profile surface roughness (σ) is acquired by:

$$\sigma = \sqrt{\frac{1}{N}(Ra_i - \mu)^2} \tag{2}$$

Then, RSDS can be acquired by:

$$\text{RSDS} = \frac{\sigma}{\mu} \tag{3}$$

The definition of RSDS develops from the relative standard deviation (RSD), which is commonly applied in many fields such as renewal theory, queueing theory, and reliability theory. RSDS provides an evaluation of the variation degree of surface roughness in the context of average surface roughness, so the value of RSDS is a dimensionless number.

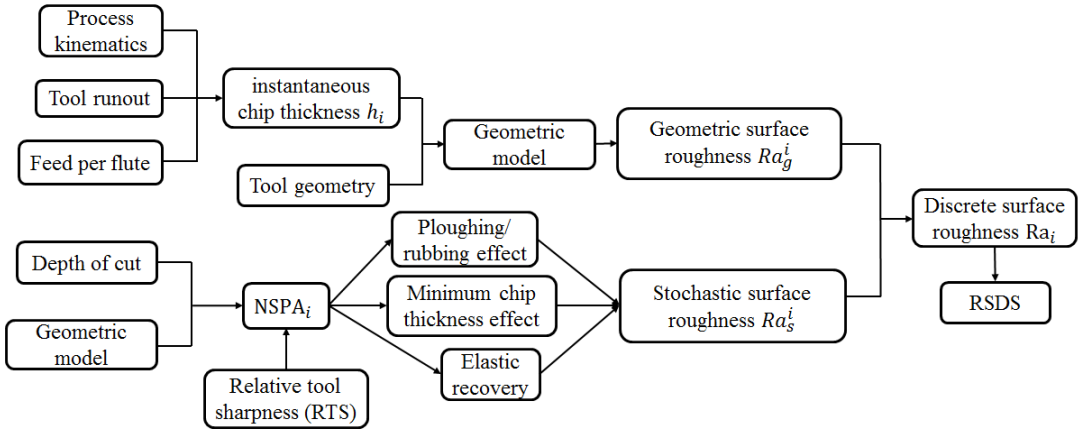

Fig. 3. Scheme of proposed model to predict RSDS.

3.2 Modelling for surface non-uniformity

The flow chart of the proposed model is illustrated in Fig. 3. Before calculating RSDS, discrete surface roughness (Ra_i) across the cross-sectional direction of micro-milled slots needs to be computed separately, and different geometric models are required to satisfy the varying instantaneous uncut chip thickness (h_i). Discrete surface roughness is the sum of geometric surface roughness (Ra_g^i) and stochastic surface roughness (Ra_s^i) at rotation angle φ_i. Geometric surface roughness is determined by the tool geometric residual marks and elastic recovery height, while stochastic surface roughness is caused by the special cutting mechanisms such as ploughing effect and minimum chip thickness effect. The workpiece material properties in the model are regarded as homogeneous and isotropic.

In Fig. 4, a chip departure point is assumed on the edge of the milling tool. Material above the point flows upwards in the direction of the negative rake angle ($-\gamma_i$) and forms a chip, while material below the point only experiences elastic-plastic deformation. Stochastic surface roughness is acquired

through calculating the normal specific ploughing amount ($NSPA_i$) that is defined as the arithmetic product between the ratio of the volume of ploughed material to the volume of total tool-workpiece contact material and the normal vector of chip flow at the rotation angle φ_i. $NSPA_i$ is derived from the specific ploughing amount (SPA) which is normally used as an index for the extent of ploughing effect [17]. The novelty of $NSPA_i$ is the integration of the relative tool sharpness (RTS), which is defined as the ratio of uncut chip thickness to the tool edge radius ($\frac{h_i}{r_e}$). $NSPA_i$ can be expressed by:

$$NSPA_i = \frac{A_p^i \cdot sin\gamma_i}{A_t^i} = \frac{A_p^i \cdot sin\gamma_i}{A_s^i + A_p^i} \tag{4}$$

where A_t^i is the total volume of tool-workpiece contact material, and A_s^i and A_p^i represents the volume of sheared material and ploughed material respectively. After the calculation of the discrete surface roughness across the whole discrete rotation angle (φ_i), RSDS can be computed based on Eq. (3).

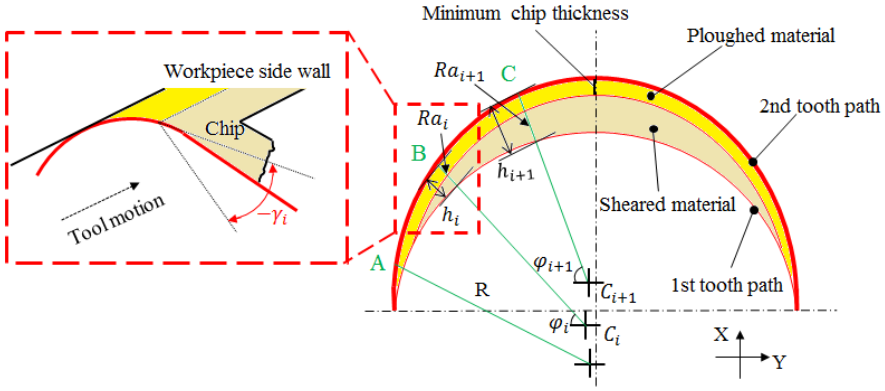

Fig. 4. Distribution of discrete surface roughness along the rotation angle.

Geometric surface roughness (Ra_g^i) is derived through calculating the value of tool residual marks and its corresponding elastic recovery height (h_e^{ij}) in the feed direction at discrete rotation angle (φ_i). Tool residual marks are formed by the superposition between previous surface profile and tool edge profile, which is determined by instantaneous uncut chip thickness (h_i) between two neighboring tool trajectories.

As shown in Fig. 5, for a two-flute micro-end milling tool, the coordinates of tool edge center (x_c^i, y_c^i) at the rotation angle (φ_i) can be expressed as:

$$\begin{cases} x_c^i = \frac{f_t}{\pi}\varphi_i + r_o \sin(\varphi_i - \pi n_f) + Rsin(\varphi_i + \delta) \\ y_c^i = r_o \cos(\varphi_i - \pi n_f) + Rcos(\varphi_i + \delta) \end{cases} \tag{5}$$

where f_t is the feed per tooth, R is the normal radius of the milling tool, n is the spindle rotation speed, n_f equals to 0 or 1 representing the ordinal number of the two cutting flutes, r_o and δ denotes the tool runout length and runout angle respectively.

Assuming φ_i is approximately equal to φ_{i+1}, the instantaneous uncut chip thickness (h_i) can be computed from Eq. (5) and simplified according to Ref. [19] as:

$$h_i = (-1)^{n_f} \cdot 2r_o[\frac{\sin(\delta)\sin(\varphi_i - \pi n_f)}{\pi R} - \cos(\delta)] + f_t[\sin(\varphi_i - \pi n_f) - \frac{f_t}{\pi R} sin(\varphi_i - \pi n_f) cos(\varphi_i - \pi n_f) + \frac{f_t}{\pi R} cos^2(\varphi_i - \pi n_f)] \quad (6)$$

where the first half of the equation reflects the process fault and the second half represents the geometrical factor of the tool edge rotation. From Eq. (6), it is known that the instantaneous uncut chip thickness periodically changes with the tool edge rotation, and increases from the sides of the micro-milled slot to the center. The maximum value of the instantaneous uncut chip thickness is reached when $\varphi_i - \pi n_f = \frac{\pi}{2}$. The maximum uncut chip thickness (h_{max}) can be expressed as:

$$h_{max} = (-1)^{n_f} \cdot 2r_o[\frac{\sin(\delta)}{\pi R} - \cos(\delta)] + f_t \quad (7)$$

Due to the variation to the uncut chip thickness with rotation angle, the geometric tool residual marks change from the sides to the center, and the dominance of ploughing effect decreases from the slot sides to the center. Consequently, it is necessary to calculate the geometric surface roughness (Ra_g^i) and stochastic surface roughness (Ra_s^i) separately based on φ_i. Considering the minimum chip thickness (h_{min}) and tool edge geometry, when $h_{max} > \sqrt{{r_e}^2 \sin^2\alpha + 2r_e h_{min} + {h_{min}}^2} + r_e sin\alpha$, there are three different intervals for each tool flute rotation with instantaneous uncut chip thickness above or less than minimum chip thickness, as see in Fig. 5 (a), (b) and (c), representing the points A, B and C in Fig. 4 respectively [17]. r_e represents tool edge radius. For Al6061, the minimum chip thickness is estimated to be $\sim 0.4r_e$ [20], and elastic recovery coefficient ρ is estimated to be 0.09 [21].

The tool edge profile (z_e^{ij}) at the discrete point x_j in the direction of φ_i can be written as:

$$z_e^{ij} = \begin{cases} -\sqrt{{r_e}^2 - (x_j - h_i)^2} & x_j > h_i - r_e \sin\alpha \\ -\tan\alpha \cdot (x_j - h_i) - \frac{r_e}{cos\alpha} & x_j \le h_i - r_e \sin\alpha \end{cases} \quad (8)$$

where α is the clearance angle of the milling tool edges. The tool geometric residential height can be computed from the residential tool edge profile z_e^{ij}.

Because of minimum chip thickness effect, it is assumed that the material under the minimum

uncut chip thickness (h_{min}) is not removed from tool edge and only experiences elastic recovery. The recovery height is according to the material elastic recovery coefficient. Considering the clearance angle of the tool edge and the minimum chip thickness, the elastic recovery height (h_e^{ij}) at φ_i direction and x_j should be calculated piecewise and can be written as:

$$h_e^{ij} = \begin{cases} 0 & 0 < x_j < r_e sin\theta_1 \\ \rho \cdot \delta(x_j) \cdot \hat{n}(x_j)(\sqrt{{x_j}^2 + (z_e^{ij})^2} - r_e) & r_e sin\theta_1 \le x_j < h_i + r_e sin\theta_1 \end{cases} \tag{9}$$

with

$$\theta_1 = \begin{cases} sin^{-1}\left(\frac{h_i}{2r_e}\right) & 0 < h_i < 2r_e sin\alpha \\ \frac{\pi}{2} - \alpha - sin^{-1}\frac{[r_e cos\alpha - tan\alpha(h_i - r_e sin\alpha)]\cdot \sin(\frac{\pi}{2}+\alpha)}{r_e} & 2r_e sin\alpha \le h_i \le h_{max} \end{cases} \tag{10}$$

and

$$\hat{n}(x_j) = \begin{cases} \frac{[x_j, z_e^{ij}]}{\sqrt{x_j^2 + (z_e^{ij})^2}} & 0 < h_i < 2r_e sin\alpha \\ \frac{[x_j - h_i, z_e^{ij}]}{\sqrt{(x_j - h_i)^2 + (z_e^{ij})^2}} & 2r_e sin\alpha \le h_i \le h_{max} \; and \; x_j > h_i - r_e \sin\alpha \\ \frac{[tan\alpha, 1]}{\sqrt{1 + tan^2\alpha}} & 2r_e sin\alpha \le h_i \le h_{max} \; and \; x_j \le h_i - r_e \sin\alpha \end{cases} \tag{11}$$

where ρ is the elastic recovery coefficient, and h_{max} can be calculated by Eq. (7), and $\hat{n}(x_j)$ is the normal vector along the tool edge, and $\delta(x_j)$ represents the coefficient of the ratio of ploughed material over the total tool cutting material at the discrete point x_j that can be expressed as:

$$\delta(x_j) = \begin{cases} 1 & r_e sin\theta_1 < x_j < r_e cos\theta_2 \\ \frac{h_{min}}{\sqrt{{x_j}^2 + {z_e^{ij}(x_j)}^2 - {r_e}^2}} & r_e cos\theta_2 \le x_j < h_i + r_e sin\theta_1 \end{cases} \tag{12}$$

with

$$\theta_2 = \begin{cases} cos^{-1}\left[\frac{h_i^2 + r_e^2 - (r_e - h_{min})^2}{2r_e h_i}\right] & 0 < h_i < r_e cos\left[sin^{-1}\frac{(r_e - h_{min})\sin(\frac{\pi}{2}-\alpha)}{r_e}\right] \\ \alpha + sin^{-1}\frac{(r_e - h_i tan\alpha - h_{min})\cdot \sin(\frac{\pi}{2}+\alpha)}{r_e} & r_e cos\left[sin^{-1}\frac{(r_e - h_{min})\sin(\frac{\pi}{2}-\alpha)}{r_e}\right] \le h_i \le h_{max} \end{cases} \tag{13}$$

Therefore, the surface height z_{ij} can be acquired through calculating the sum of the residential tool edge profile z_e^{ij} and the elastic recovery height h_e^{ij}. z_{ij} is written as:

$$z_{ij} = z_e^{ij} + h_e^{ij} \tag{14}$$

The geometric surface roughness in φ_i direction is defined as the arithmetic mean value of the surface profile and can be calculated from the surface profile height z(x) by the expression Ref. [17]

$$Ra_g^i = \frac{1}{l_x}\int_0^{l_x}|z(x)|dx \approx \frac{1}{\mathrm{M}}\sum_{j=0}^{j=\mathrm{M}}|z_{ij}| \tag{15}$$

where l_x is the sample length and M is the number of sample points.

The stochastic surface roughness represents the destruction of the micro-milled surface by ploughing effect. For point A in Fig. 4, its corresponding geometric model is shown in Fig 5. (a). The uncut chip thickness at A is less than the minimum chip thickness, so there are no chips formed at this point. The total tool-workpiece contact volume is classified as ploughed material at A. Calculated by Eq. (4), NSPA_i at point A can be written as:

$$\mathrm{NSPA}_i = sin\gamma_i \qquad (h_i < h_{min}) \tag{16}$$

The calculation of negative rake angle $-\gamma_i$ is given in Ref [22] using the average method as:

$$\gamma_i = \left[\left(1-\frac{h_i}{r_e}\right)\times sin^{-1}\left(1-\frac{h_i}{r_e}\right)+\sqrt{1-\left(1-\frac{h_i}{r_e}\right)^2}-\frac{\pi}{2}\right]/\frac{h_i}{r_e} \tag{17}$$

where h_i is the instantaneous uncut chip thickness at rotation angle φ_i. Because of the introduction of γ_i into calculating the specific ploughing amount SPA, the effect of relative tool sharpness (RTS) on the variation of surface generation mechanisms is incorporated into the computation of surface roughness.

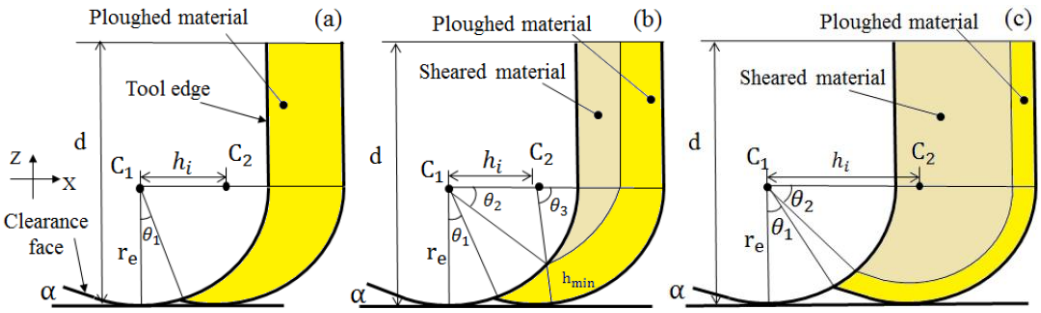

Fig. 5. Geometry models of cutting regions with uncut chip thickness (a) lower than minimum chip thickness, (b) beyond minimum chip thickness but without influence of clearance angle and (c) uncut chip thickness influenced by clearance angle.

At point B in Fig. 4, the instantaneous uncut chip thickness is beyond the minimum chip thickness, but not long enough to reach the clearance angle. When $h_i < 2r_e sin\alpha$, the whole cutting edge can be regarded as a round edge. Considering the influence of ploughing effect from both sidewall and tool edge bottom, the volume of total tool-workpiece contact material (A_t^i) at instantaneous uncut chip thickness (h_i) can be written as:

$$A_t^i = r_e^2 \cdot \theta_1 + 0.5 h_i r_e cos\theta_1 + (d - r_e)h_i \qquad (h_{min} < h_i < 2r_e sin\alpha) \tag{18}$$

where d is the depth of cut, and θ_1 is given as Eq. (10). According to the geometric relation, the volume of ploughed material (A_p^i) at point B can be expressed as:

$$A_p^i = A_t^i - (r_e - h_{min})^2 \cdot \theta_3 + r_e^2 \cdot \theta_2 - \frac{h_i}{2}(r_e - h_{min})sin\theta_3$$

$$-(d - r_e)(h_i - h_{min}) \qquad (h_{min} < h_i < 2r_e sin\alpha) \tag{19}$$

where θ_2 can be computed from Eq. (13), and θ_3 can be given as:

$$\theta_3 = \pi - cos^{-1}\frac{h_i^2 + (r_e - h_{min})^2 - r_e^2}{2h_i(r_e - h_{min})} \tag{20}$$

In a comparable way, the calculation of the volume of total tool-workpiece contact material (A_t^i) and the volume of ploughed material (A_p^i) at point C in Fig. 5 and Fig. 6 (c) should take into consideration the clearance angle and the round cutting edge, according to Eq. (8). It can be written as:

$$A_t^i = r_e^2 \cdot \theta_1 - \frac{h_i^2 tan\alpha}{2} - \frac{r_e sin\theta_1 (r_e - h_i tan\alpha)}{2} + dh_i \qquad (2r_e sin\alpha < h_i < h_{max}) \tag{21}$$

when $2r_e sin\alpha < h_i < r_e cos\left[sin^{-1}\frac{(r_e - h_{min})\sin(\frac{\pi}{2} - \alpha)}{r_e}\right]$, A_p^i can be computed by Eq. (19) and when $r_e cos\left[sin^{-1}\frac{(r_e - h_{min})\sin(\frac{\pi}{2} - \alpha)}{r_e}\right] \le h_i < h_{max}$, A_p^i can be computed as:

$$A_p^i = A_t^i - (r_e - h_{min})^2\left(\frac{\pi}{2} + \alpha\right) - \frac{(r_e - h_{min})^2 sin\alpha \cdot cos\alpha}{2} + \frac{[h_i - (r_e - h_{min})sin\alpha]^2}{2}tan\alpha$$

$$+(d - r_e)(h_i - h_{min}) + r_e^2 \cdot \theta_2 - (r_e - h_{min})[h_i - (r_e - h_{min})sin\alpha]cos\alpha$$

$$+\frac{r_e sin\theta_1}{2}[(r_e - h_{min})(cos\alpha + sin\alpha \cdot tan\alpha) - h_i tan\alpha] \tag{22}$$

Then, based on Eqs. (18), (19), (21) and (22), NSPA_i for point B and C can be calculated by Eq. (4). According to the research result by Liu et al. [17], the stochastic surface roughness can be modeled as a function of specific ploughed amount. Stochastic surface roughness Ra_s^i at φ_i can be given as:

$$Ra_s^i = K(\mathrm{NSPA}_i)^n \tag{23}$$

where K and n are the material related coefficients, which are calculated based on the L25 Taguchi experimental results to be 0.17 and 0.83 respectively. The calculating method is presented in detail in Ref [23].

After calculating the surface roughness (Ra_i) in the feed direction at φ_i, the relative standard deviation of the average surface roughness can be calculated, based on the definition as:

$$\mathrm{RSDS} = \frac{\sqrt{\frac{1}{N}\sum_{i=1}^{i=\mathrm{N}}\left(Ra_i - \frac{1}{I}\sum_{i=1}^{i=\mathrm{N}} Ra_i\right)^2}}{\frac{1}{\mathrm{N}}\sum_{i=1}^{i=\mathrm{N}} Ra_i} \tag{24}$$

with

$$Ra_i = Ra_g^i + Ra_s^i \tag{25}$$

where N is the number of sampling points along the cross-sectional direction of micro-milled slots.

4. Results and discussion

4.1 Surface non-uniformity

Fig. 6 illustrates the modelling for the variation of surface generation mechanisms at different regions. The A, B and C in Fig. 6 represents the tool-workpiece engagement point, slot center and disengagement point respectively and their corresponding SEM images is shown in Fig. 7 (a), (b) and (c). It is learned from the model that significant ripple marks and cracks were simultaneously observed at the tool-workpiece engagement and disengagement points. In contrast, smooth residual tool marks can be observed in the center of the slot. The different surface topography at different intervals indicates different surface roughness. As shown in Fig. 8, both the simulated and the experimental surface roughness in the cross-sectional direction were not constant, but decreased gradually from the sides to the center. It is therefore apparent that a micro-milled surface presents serious non-uniformity in the cross-sectional direction.

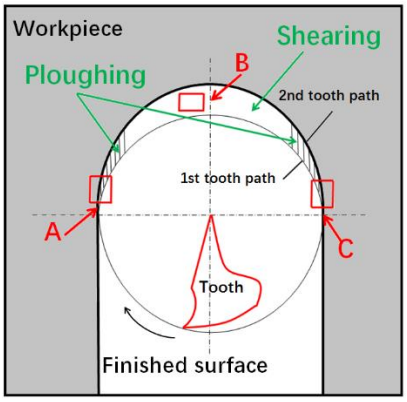

Fig. 6. Modelling for the variation of surface generation mechanisms from the upper view of tool track.

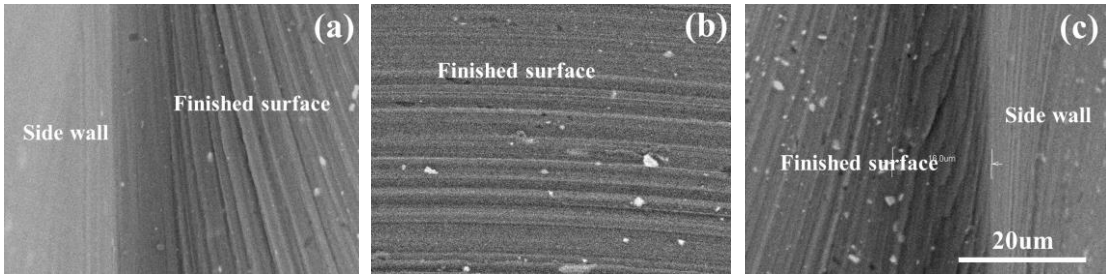

Fig. 7. SEM images at (a) engagement point (b) slot center (c) disengagement point.

As learned from the proposed model, the instantaneous uncut chip thickness periodically changes with tool rotation. Chips are hardly formed at the tool-workpiece engagement and disengagement points due to the low uncut chip thickness. The workpiece material is machined under plastic or elastic

deformation. As shown in Fig. 8, the higher surface roughness on the sides is mainly caused by the ploughing induced plastic dissipation energy at the grain boundary [10]. When the height of the material stack is beyond the value of minimum chip thickness, the shear band forms gradually along the tool-rotating track. Much lower surface roughness is found in the center, because the surface generation mechanism transfers from plastic deformation/ploughing to shearing. Hence, the effect of the variation of uncut chip thickness and its induced variation of surface generation mechanisms on surface roughness is significant in micro-milling, which leads to serious surface non-uniformity.

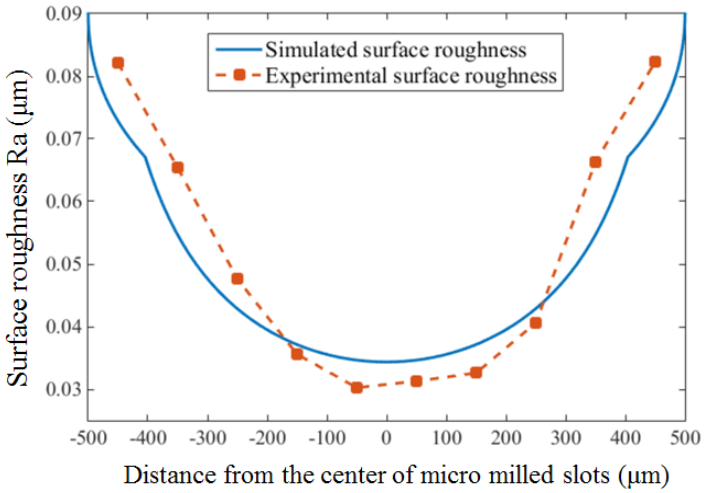

Fig. 8. Surface roughness at different sub-regions across the cross-sectional direction of the micro-milled slot with feed rate at 1.2 μm/flute and depth of cut at 30μm.

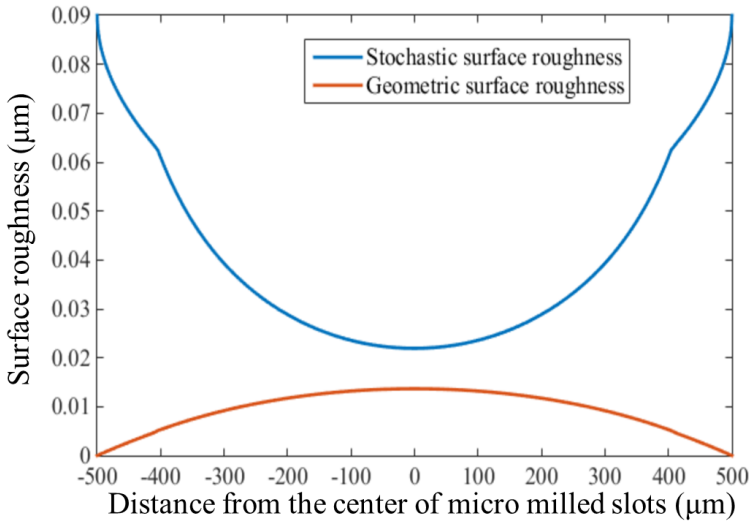

Fig. 9. The distribution of geometric surface roughness and stochastic surface roughness at feed rate 0.8μm/flute and 40μm depth of cut.

Furthermore, it should be noted from the Fig. 9 that the geometric surface roughness and

stochastic surface roughness are not invariant, which is opposite to the trend from slot sides to the center. The variation of geometric surface roughness is caused by the effect of the clearance angle of the micro-milling tool, as illustrated in Eq. (8). In contrast, the decreasing trend of stochastic surface roughness from slot sides to the center is because of the reduction of NSPA_i with increasing uncut chip thickness. The reduction of NSPA_i indicates a lower negative rake angle and lower ratio of ploughed material to total tool contact material, as shown by Eq. (4), which means less ploughing mechanism and more shearing mechanism in material removal. As the percentage of stochastic surface roughness is much larger than that of geometric surface roughness in micro-milling, the micro-milled surface quality is mainly influenced by the stochastic surface roughness, which causes the non-uniformity of micro-milled surfaces.

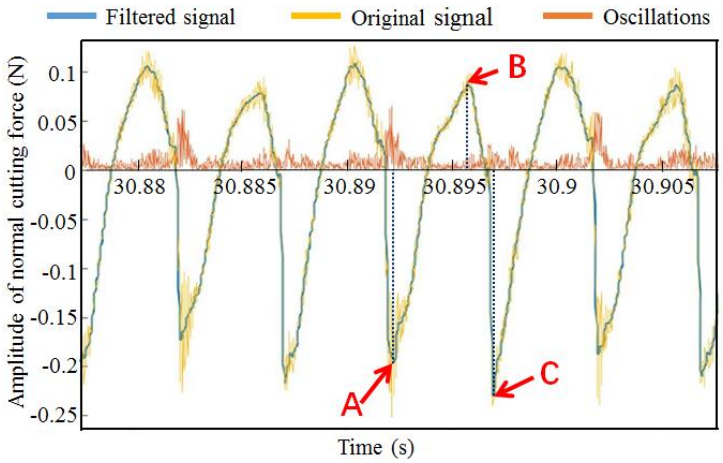

Fig. 10. Amplitude of cutting force oscillations at 1.2μm/flute.

The variation of surface generation mechanisms can be further elaborated through analyzing the cutting force oscillations, as shown in Fig. 10. The amplitude of oscillations (the red line) is calculated by subtracting the value of filtered force (the blue line) from the original cutting force (the yellow line). It is clear that the amplitude of oscillations obviously changed in sync with tooth passing frequency. A high peak value of oscillation was distributed at each tool-workpiece engagement and disengagement points (A and C points), which is caused by the severe shocking and ploughing effect when the milling tool contacts and leaves the workpiece. This elevated level of cutting force oscillations also corresponds to the severe surface defects at tool-workpiece engagement and disengagement points as shown in Fig. 7 (a) and (c). In contrast, a relatively low value of oscillation is distributed at point B, corresponding to the smooth surface texture in the slot center, as shown in Fig. 7 (b). This is because of

the formation of shear band with increasing uncut chip thickness. The lowest cutting force oscillation is achieved near the maximum uncut chip thickness point. Consequently, the surface generation mechanism in micro-milling periodically transforms from ploughing to shearing during each tool flute rotation, and there is an obvious ploughing interval and shearing interval in the cross-sectional direction of micro-milled slots.

Similar conclusions have been drawn in previous studies. According to Fernando et al. [5], there are six chip formation intervals along each tool-workpiece engagement, corresponding to the variation of cutting mechanism. These intervals are well defined by the tool rotation angle when the cutting thickness reaches some specific dimension, such as minimum chip thickness and tool edge radius. Through measuring the cutting force signals and analyzing the dynamic properties of micro-milling, Özel concluded that micro-milling is dominated by a continuous shift between cutting and ploughing mechanisms [24].

The results of ANOVA analysis on RSDS are presented in Table 3. The P-value of feed rate and depth of cut is less than the adopted significance level (α=0.05). Therefore, it is observed that feed rate and depth of cut present a pronounced influence on the RSDS (at 95% confidence level). However, spindle speed has very little effect on RSDS.

Table 3. ANOVA of surface non-uniformity.

ANOVA for RSDS					
Parameter	DOF	SS(adj.)	MS(adj.)	F	P
Spindle speed	4	0.004986	0.001247	1.46	0.275
Feed rate	4	0.038705	0.009676	11.33	0.000
Dopth of cut	4	0.020590	0.005148	6.03	0.007
Residual	12	0.010249	0.000854		
Total (corrected)	24	0.074531			
S=0.0292251; R-Sq=86.25%; R-Sq(adj.)=72.50%					

Overall, the non-uniform surface is mainly caused by the periodic transformation of surface generation mechanisms from ploughing to shearing, which can be illustrated by the variation of the surface roughness and the periodic cutting force oscillations. Through ANOVA, it is leaned that spindle speed has no obvious relationship with surface non-uniformity, while both feed rate and depth of cut significantly influence surface non-uniformity. The effect of feed rate and depth of cut on RSDS is further illustrated based on the SN ratio analysis below.

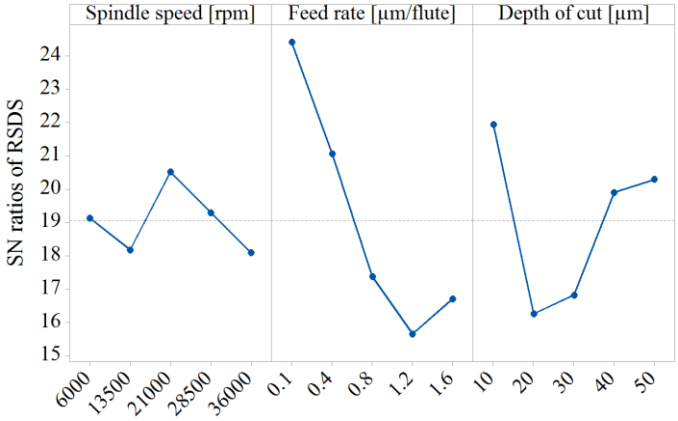

Fig. 11. Analysis of means plot for SN ratios of RSDS.

4.2 Feed rate effect

As shown in Fig. 11, the SN ratio of RSDS decreased dramatically with feed rate from 0.1µm/flute to 1.2µm/flute. Namely, when the feed rate is lower than 1.2µm/flute, the micro-milled surface non-uniformity deteriorated with increase of feed rate. As shown in Fig. 12, the 2D cross-sectional surface texture at different feed rates exhibited smooth surface texture in the slot center representing the shearing interval. By contrast, significantly high peaks and valleys were distributed on both up-milling and down-milling sides representing the ploughing interval. Meanwhile, through comparing the 3D characteristic of micro-milled surfaces at different feed rates, it is also observed that the generated surface topographies became increasingly non-uniform with increasing feed rate. Therefore, based on the ANOVA and SN ratio analysis, it is demonstrated that RSDS proposed in this paper can well reflect the variation of micro-milled surface non-uniformity.

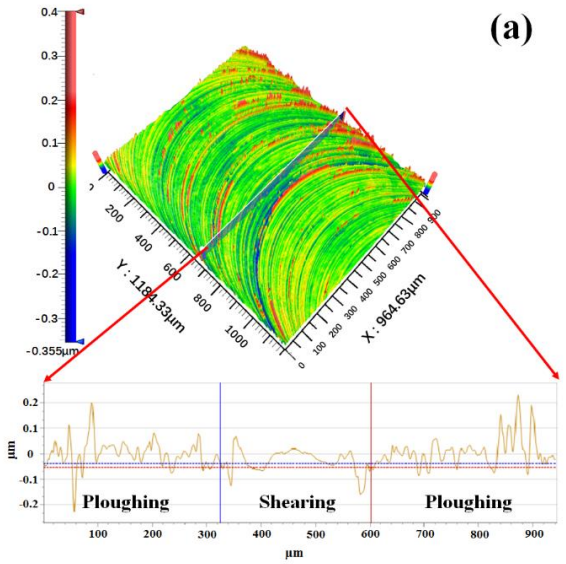
(a)
Y: 1184.33µm
X: 964.63µm
-0.355µm
Ploughing
Shearing
Ploughing
µm

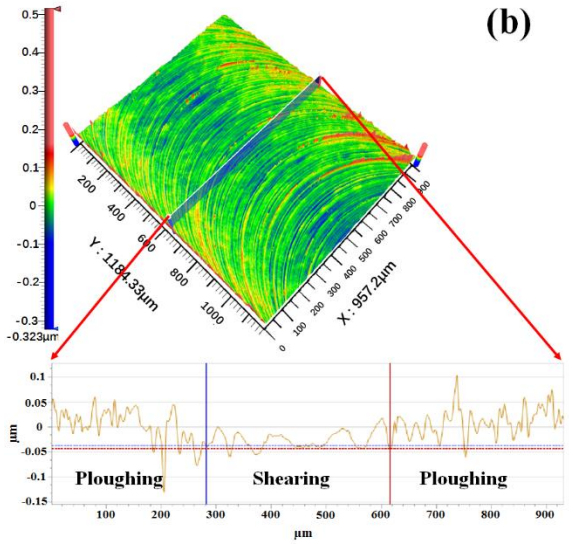
(b)
Y: 1184.33µm
X: 957.2µm
-0.323µm
Ploughing
Shearing
Ploughing
µm

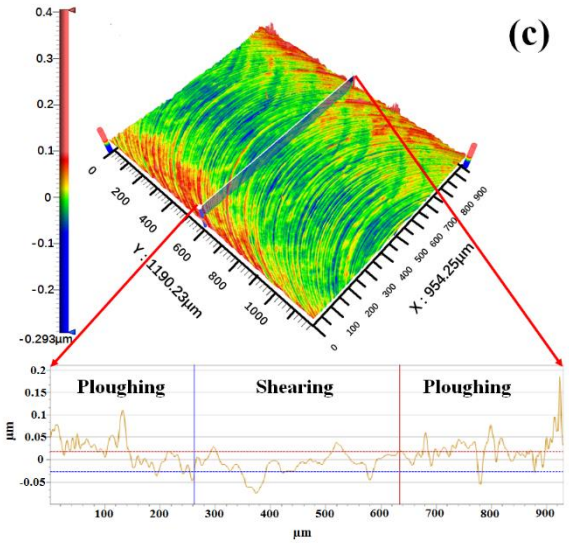
(c)
Y: 1190.23µm
X: 954.25µm
-0.293µm
Ploughing
Shearing
Ploughing
µm

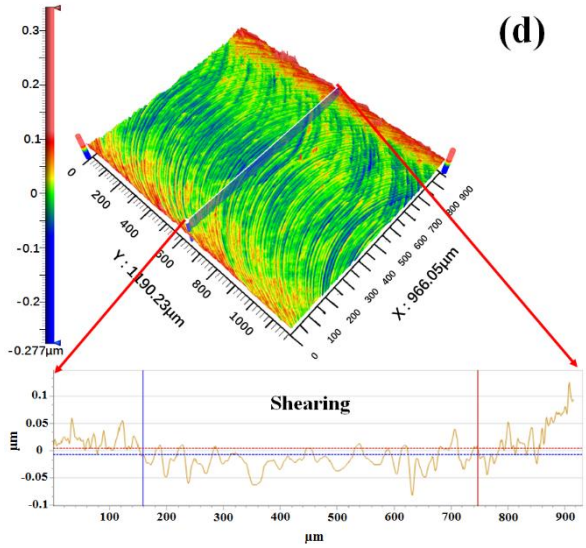

Fig. 12. Finished surface characteristic and cross-sectional 2D profile with depth of cut at 10µm and (a) feed rate at 0.1µm/flute, (b) 0.4µm/flute, (c) 0.8µm/flute, (d) 1.2µm/flute.

The shearing interval elongated with increasing feed rate, as shown in Fig. 13. From Eq. (7), the maximum uncut chip thickness in the center of micro-milled slots is in direct proportion to feed rate. Hence, increasing feed rate dramatically improves the cutting conditions in the center of the slot. It was learnt from the proposed model that the larger the feed rate, the longer the interval with uncut chip thickness beyond the minimum chip thickness in the slot center. In contrast, the uncut chip thickness remains at zero at both tool-workpiece engagement and disengagement points regardless of the variation of feed rate. Thus, the surface generation mechanism near the center of the slot is much more sensitive to feed rate than that near both engagement and disengagement points. Slightly increasing feed rate can improve the surface quality in the center of the slot, while the closer to the sides, the weaker this improvement became. Therefore, the growing length of shearing interval is the main reason why surface non-uniformity deteriorates with increasing feed rate.

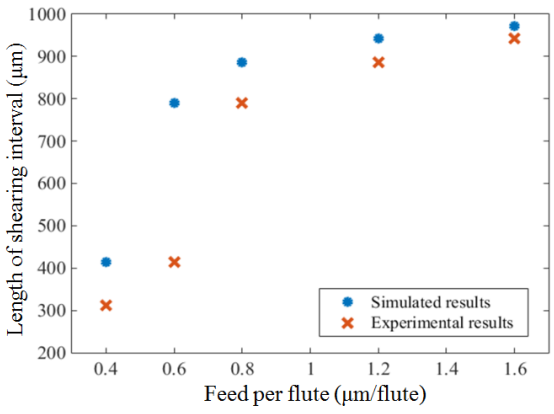

Fig. 13. Variation of simulated and experimental length of shearing interval.

Based on the proposed mathematical model, the distribution of simulated surface roughness in the cross-sectional direction becomes increasingly non-uniform with increase of feed rate (Fig. 14), which presents the same tendency as the experiment results. The simulated surface roughness in the vicinity of the slot center decreases with feed rate, while surface roughness remains constant on the sides at different feed rates. Additionally, there exists an obvious threshold valve between the ploughing interval and shearing interval both in the experiments and the simulation results, as the transforming points shown in Fig. 12 and Fig. 14. This means that there exists a sharp switch between ploughing and shearing interval.

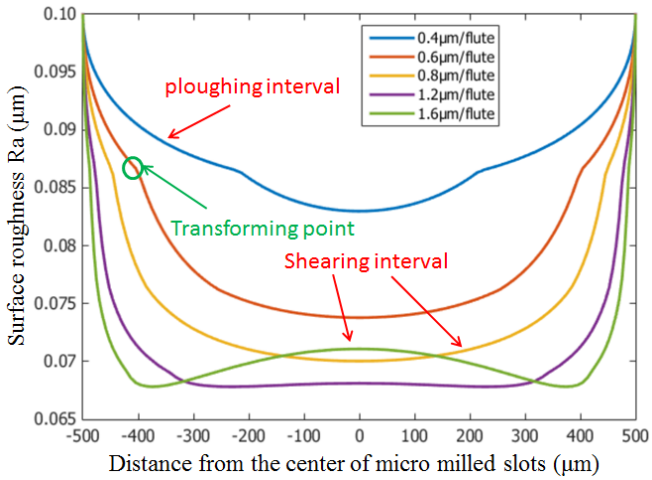

Fig. 14. Distribution of simulated surface roughness in the cross-sectional direction of micro-milled slots with different feed rates.

An increasing length of shearing interval indicates a greater degree of variation of surface generation mechanisms and an increasing deterioration in surface uniformity. For example, the increment of uncut chip thickness with tool rotation at 0.4μm/flute is much lower than that at 1.2μm/flute, so the distribution of surface roughness at 0.4μm/flute presents better uniformity. However, the surface roughness at 0.4μm/flute is also much higher due to the prevalence of ploughing effect at low feed rate. Meanwhile, the increasing length of shearing interval at a higher feed rate reduces the average surface roughness, which in turn makes the non-uniformity deteriorate. When feeding at 1.6 μm/flute or above, the micro-milling process switches to the macro-milling process. The dominant factors affecting average surface roughness transforms to geometric tool marks. It is speculated that RSDS remains constant in the macro-milling process.

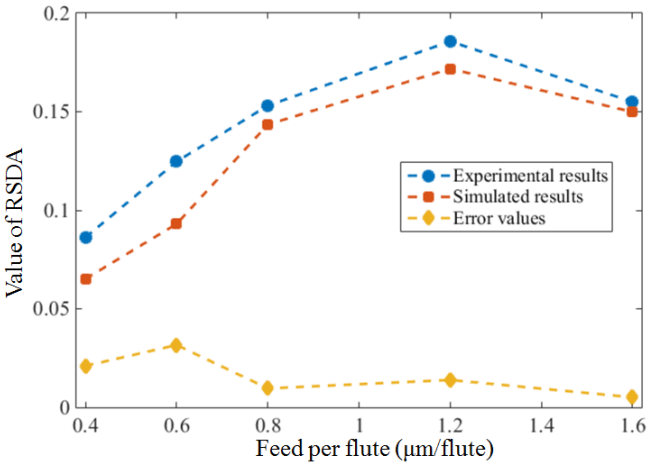

Fig. 15. Cooperation of simulated and calculated RSDS with increasing chip load.

Fig. 15 compares the results of RSDS from the Taguchi experiments and the mathematical model proposed in this study. It is seen that the calculated RSDS matches the experiment results well in the varying tendencies. The mean estimating error is 16.35%. The main reason for the error is attributed to the limited number of sampling intervals when calculating the experimental RSDS.

It is obvious that the estimating error at low feed rates is much higher than that at higher feed rates. This is because the effects of the dynamic factors on surface quality at low feed rates are much higher than that at higher feed rates. Meanwhile, the relative lower simulated RSDS as compared with the experimental results is caused by the neglect of micro cracks and the extrusion marks on the sides. In addition, the elastic recovery in the model is regarded as a linear process, which also affects the accuracy of the model.

Overall, the change of relative length between shearing interval and ploughing interval with feed rate is caused by the different sensitivity to the uncut chip thickness increment between the center of the slot and the tool-workpiece engagement and disengagement points. This resulting in increasingly severe surface non-uniformity and large RSDS.

4.3 Depth of cut effect

Apart from depth of cut at 10μm, the SN ratios of RSDS increased gradually with increasing depth of cut, as shown in Fig. 11. Namely, the surface non-uniformity was the worst at 20μm, and improved with increasing depth of cut. From Fig. 16, it is clear that the 3D topography of finished surface at 20μm presents obviously more non-uniformity than that at 30μm and 40μm. Higher tool

marks were distributed on the sides of the slot at 20µm. The better surface uniformity at 10µm is due to the severe ploughing effect spreading along the whole tool-rotating track. Comparing Fig 12. (a) and Fig. 16 (a), the 3D topography of finished surface at 10µm showed a more plane shape than that at 20µm, but the surface roughness at 10µm is also much higher. The variation of surface generation mechanisms at low depth of cut is not as obvious as that at higher depth of cut, so the surface non-uniformity at 10µm is better than others.

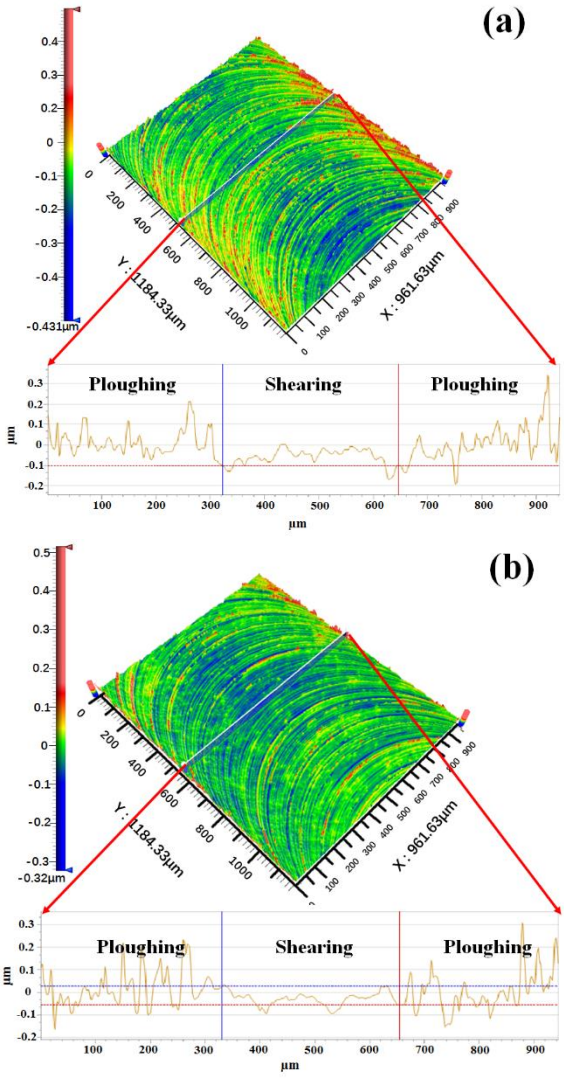

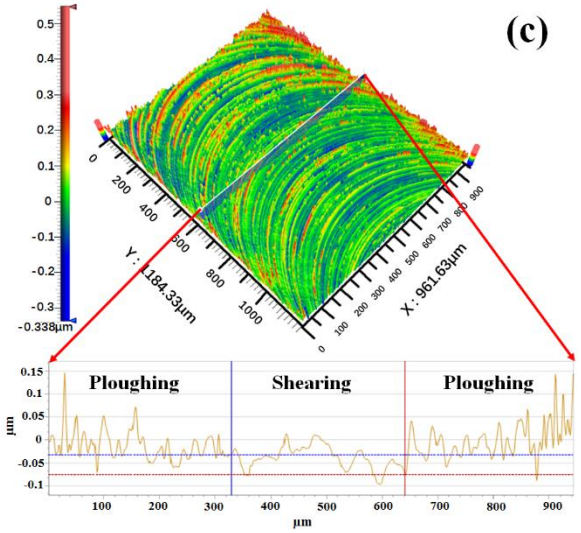

Fig. 16. Surface topography at (a) 20μm (b) 30μm (c) 40μm feed rate 0.1μm/flute.

The effect of depth of cut on surface non-uniformity can be well illustrated through comparing the different 2D cross-sectional profiles with depth of cut at 20μm, 30μm and 40μm in Fig. 16. Differing from feed rate, the length of shearing interval in the center of the micro-milled slots was almost unchanged at different depth of cuts. The shearing interval length with depths of cut at 20μm, 30μm and 40μm are equal to 323μm, 324μm and 311μm respectively. Based on the proposed mathematical model, the distribution of simulated surface roughness along the cross-sectional direction at different depth of cuts is shown in Fig. 17. It is seen that the transforming point is fixed at different depth of cuts, which indicates a fixed length of shearing interval. This is because when the value of minimum chip thickness is constant, the transforming point between ploughing to shearing is mainly determined by the increment of uncut chip thickness. As learned from Eq. (6), the instantaneous uncut chip thickness is the function of rotation angle φ_i. The increment of uncut chip thickness is mainly determined by feed rate, so depth of cut has no direct relationship with shearing interval length. As a result, it is learnt that the change of RSDS with depth of cut is not caused by the change of relative length of shearing interval, as with feed rate.

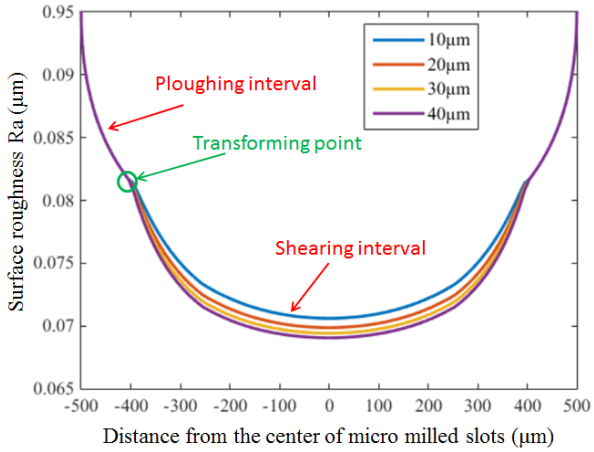

Fig. 17. The distribution of simulated surface roughness with different depth of cuts.

However, the surface roughness distributed in the shearing interval decreases with increasing depth of cut, as shown in Fig. 17. The comparison between simulated and experimental results of average surface roughness in shown in Fig. 18. It is seen that the average surface roughness decreased with increasing depth of cut, which means better cutting conditions are achieved at a higher depth of cut. As mentioned earlier, average surface roughness is mainly determined by the stochastic surface roughness. Stochastic surface roughness decreases with increasing depth of cut because increasing depth of cut reduces the ratio of the volume of ploughed material to the volume of total tool-workpiece contact material further to reduce NSPA_i. The influence weakens gradually at higher depth of cut, as the effect of tool edge radius on surface generation declines at higher depth of cut. Hence, the variation of NSPA_i is principally determined by uncut chip thickness when depth of cut is beyond a critical value. Therefore, even though the feed rate is fixed, ploughing effect diminishes at higher depth of cut. Decreased average surface roughness indicates not only better cutting condition but also unremarkable difference between the surface roughness at shearing interval and ploughing interval. The decreasing RSDS with depth of cut is therefore caused by the improvement of cutting conditions.

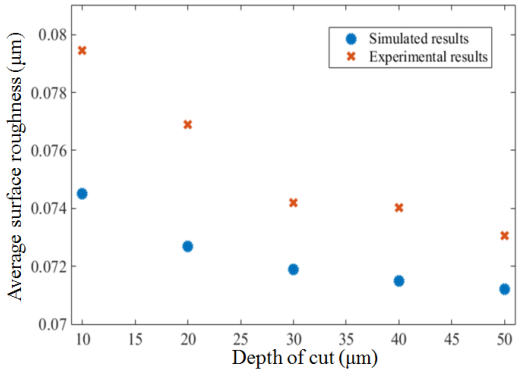

Fig. 18. Mean value of surface roughness with increasing depth of cut.

Overall, depth of cut does not influence the relative length of shearing interval and ploughing interval. However, the decreasing trend of average surface roughness with depth of cut leads to the increasing SN ratios of RSDS from 20μm to 40μm.

5.Conclusions

This paper presents an experimental and theoretical study of micro-milled surface non-uniformity under the variation of surface generation mechanisms. A novel relative standard deviation of surface roughness (RSDS) method is proposed to evaluate the micro-milled surface non-uniformity. Meanwhile, a mathematical model considering relative tool sharpness (RTS) is developed to predict surface non-uniformity. The variation of surface generation mechanisms and the effect of machining parameters on surface non-uniformity in micro-milling is discussed theoretically and experimentally. The study's key conclusions are as follows:

(1) The dominant surface generation mechanism for micro-milling periodically transforms from ploughing to shearing, which induces periodic cutting force oscillations and severely non-uniform surface. Although cutting speed shows no apparent connection with surface uniformity, both feed rate and depth of cut have a pronounced influence on surface uniformity.

(2) The 3D characteristic and the 2D cross-sectional profile of a non-uniform surface exhibit higher surface roughness on the sides and lower surface roughness in the center. The non-uniform surface is mainly attributed to the variation of stochastic surface roughness as the ratio of stochastic surface roughness is much larger than that of geometric surface roughness.

(3) The length of shearing interval in the slot center is mainly determined by feed rate. The deterioration of surface uniformity with feed rate is mainly due to the different sensitivity to the uncut chip thickness increment between the slot center and the sides.

(4) Different from feed rate, depth of cut has no influence on ratio between the length of shearing interval and ploughing interval. The reduction of micro-milled surface non-uniformity with increasing depth of cut is mainly caused by the reduction of average surface roughness.

(5) The effectiveness of RSDS in evaluating surface non-uniformity is demonstrated theoretically and experimentally. The proposed model well predicts the surface non-uniformity and the variation of surface roughness in the cross-sectional direction of micro-milled slots.

Acknowledgement

This work was supported partially by the Research Committee of The Hong Kong Polytechnic University (Project Code: RUNS).

References

[1] J.P. Davim, Modern mechanical engineering, Springer, 2014.
[2] X. Lai, H. Li, C. Li, Z. Lin, J. Ni, Modelling and analysis of micro scale milling considering size effect, micro cutter edge radius and minimum chip thickness, International Journal of Machine Tools and Manufacture, 48 (2008) 1-14.
[3] K. Woon, M. Rahman, Extrusion-like chip formation mechanism and its role in suppressing void nucleation, CIRP Annals-Manufacturing Technology, 59 (2010) 129-132.
[4] A.C. Ramos, H. Autenrieth, T. Strauß, M. Deuchert, J. Hoffmeister, V. Schulze, Characterization of the transition from ploughing to cutting in micro machining and evaluation of the minimum thickness of cut, Journal of Materials Processing Technology, 212 (2012) 594-600.
[5] F.B. de Oliveira, A.R. Rodrigues, R.T. Coelho, A.F. de Souza, Size effect and minimum chip thickness in micromilling, International Journal of Machine Tools and Manufacture, 89 (2015) 39-54.
[6] A. Mian, N. Driver, P. Mativenga, Identification of factors that dominate size effect in micro-machining, International Journal of Machine Tools and Manufacture, 51 (2011) 383-394.
[7] M.B. Jun, R.E. DeVor, S.G. Kapoor, Investigation of the dynamics of microend milling—part II: model validation and interpretation, Journal of manufacturing science and engineering, 128 (2006) 901-912.
[8] J. Outeiro, V. Astakhov, The role of the relative tool sharpness in modelling of the cutting process, in: Proceedings of the 8th CIRP international workshop on modeling of machining operations, 2005, pp. 517-523.
[9] M.A. Rahman, M.R. Amrun, M. Rahman, A.S. Kumar, Variation of surface generation mechanisms in ultra-precision machining due to relative tool sharpness (RTS) and material properties, International Journal of Machine Tools and Manufacture, 115 (2017) 15-28.
[10] S. Filiz, C.M. Conley, M.B. Wasserman, O.B. Ozdoganlar, An experimental investigation of micro-machinability of copper 101 using tungsten carbide micro-endmills, International Journal of Machine Tools and Manufacture, 47 (2007) 1088-1100.
[11] M. Arif, M. Rahman, W.Y. San, An experimental investigation into micro ball end-milling of silicon, Journal of Manufacturing Processes, 14 (2012) 52-61.
[12] M. Arif, M. Rahman, W.Y. San, Ultraprecision ductile mode machining of glass by micromilling process, Journal of Manufacturing Processes, 13 (2011) 50-59.
[13] V. Sooraj, J. Mathew, An experimental investigation on the machining characteristics of microscale end milling, The International Journal of Advanced Manufacturing Technology, 56 (2011) 951-958.
[14] A. Simoneau, E. Ng, M. Elbestawi, Surface defects during microcutting, International Journal of Machine Tools and Manufacture, 46 (2006) 1378-1387.
[15] E. Uhlmann, S. Piltz, K. Schauer, Micro milling of sintered tungsten‐copper composite

materials, Journal of Materials Processing Technology, 167 (2005) 402-407.
[16] R.E. DeVor, S.G. Kapoor, On the modeling and analysis of machining performance in micro-endmilling, Part I: Surface generation, J. Manuf. Sci. Eng., 126 (2004) 685-694.
[17] X. Liu, R.E. DeVor, S.G. Kapoor, Model-based analysis of the surface generation in microendmilling—part I: model development, Journal of manufacturing science and engineering, 129 (2007) 453-460.
[18] A.A. Elkaseer, S.S. Dimov, K.B. Popov, M. Negm, R. Minev, Modeling the material microstructure effects on the surface generation process in microendmilling of dual-phase materials, Journal of Manufacturing Science and Engineering, 134 (2012) 044501.
[19] W. Bao, I. Tansel, Modeling micro-end-milling operations. Part II: tool run-out, International Journal of Machine Tools and Manufacture, 40 (2000) 2175-2192.
[20] X. Liu, R. DeVor, S. Kapoor, An analytical model for the prediction of minimum chip thickness in micromachining, Journal of manufacturing science and engineering, 128 (2006) 474-481.
[21] R.E. DEVOR, S.G. KAPOOR, CUTTING MECHANISMS AND THEIR INFLUENCE ON DYNAMIC FORCES, VIBRATIONS AND STABILITY IN MICRO-ENDMILLING.
[22] X. Wu, L. Li, M. Zhao, N. He, Experimental investigation of specific cutting energy and surface quality based on negative effective rake angle in micro turning, The International Journal of Advanced Manufacturing Technology, 82 (2016) 1941-1947.
[23] X. Liu, R.E. DeVor, S.G. Kapoor, Model-based analysis of the surface generation in microendmilling—part II: experimental validation and analysis, Journal of manufacturing science and engineering, 129 (2007) 461-469.
[24] T. Özel, X. Liu, A. Dhanorker, Modelling and simulation of micro-milling process, in: 4th International Conference and Exhibition on Design and Production of Machines and Dies/Molds, 2007, pp. 21-23.